Journal of Alloys and Compounds 768 (2018) 88–96

Contents lists available at ScienceDirect

Journal of Alloys and Compounds

journal homepage: http://www.elsevier.com/locate/jalcom

Constituent constraining effects on the microstructural evolution, ductility, and fracture mode of crystalline/amorphous nanolaminates

Yaqiang Wang [a, b], Daniel Kiener [b], Xiaoqing Liang [a], Jianjun Bian [a], Kai Wu [a], Jinyu Zhang [a, *], Gang Liu [a, **], Jun Sun [a, ***]

[a] State Key Laboratory for Mechanical Behavior of Materials, Xi'an Jiaotong University, Xi'an, 710049, China
[b] Department Materials Physics, Montanuniversität Leoben & Erich-Schmid-Institute for Materials Sciences, Austrian Academy of Science, Jahnstr. 12, A-8700, Leoben, Austria

ARTICLE INFO

Article history:
Received 18 April 2018
Received in revised form
6 July 2018
Accepted 15 July 2018
Available online 19 July 2018

Keywords:
Crystalline/amorphous nanolaminates
Crystallization
Ductility
Constraining effect
Fracture mode

ABSTRACT

Manipulation of the microstructural evolution to achieve controllable deformation and fracture behaviors in crystalline/amorphous nanolaminates is a grand challenge from the perspective of constraining effects of a crystalline on an amorphous phase. In this work, crystalline/amorphous Ag/Cu-Zr and Mo/Cu-Zr nanolaminates were respectively prepared by using magnetron sputtering. The microstructural evolution, tensile ductility, and fracture mode were investigated within a wide range of modulation ratio η (the thickness ratio of amorphous to crystalline layer) from 0.1 to 9.0. The Ag/Cu-Zr nanolaminates showed the tensile ductility firstly decreased and subsequently increased with raising η, leaving a minimum value at the critical η^* of ~1.0. The fracture mode was accordingly transformed from shearing to opening. However, the Mo/Cu-Zr nanolaminates exhibited a different η-dependence where the tensile ductility monotonically increased with η, with fracture mode unchanged as opening. The strong constituent effect on the deformation and fracture of crystalline/amorphous nanolaminates was rationalized in light of the deformation-induced devitrification behaviors in the amorphous layers, which was tuned by the constituent-dependent elastic modulus mismatch and the amorphous layer thickness. Furthermore, the devitrification behaviors were qualitatively interpreted in terms of the image force between constituents and the stress field of a dislocation. These findings manifest a microstructural design by controlled constituents to achieve enhanced mechanical properties in the crystalline/amorphous nanolaminates.

1. Introduction

The amorphous microstructure with short-to-medium-range ordering in metallic glasses (MGs) underlies their desirable merits, e.g. high strength and large elasticity on one hand [1,2], and their fatal drawbacks, e.g. limited tensile ductility and thermodynamically metastable nature on the other hand [3–5]. The near-zero tensile ductility at ambient temperature caused by macroscopically localized shear bands (SBs) associated with strain softening remarkably impede exploitation of their excellent mechanical strength as engineering materials. Therefore, conferring great ductility on MGs without sacrificing their high strength is a grand challenge for structural applications. Tremendous efforts in recent years have been devoted to enabling MGs to exhibit a visible tensile ductility [6–8], among which one potential method is synthesizing the MG-matrix composites [9]. Embedding an ordered crystalline phase into the disordered amorphous matrix has been revealed, in some circumstances, to improve the ductility of the MG composite by confining the inhomogeneous shear banding and uniformizing the spatial distribution of plasticity [6,10], but also in some other cases to achieve the enhancement in strength [9,11].

A representative example is the addition of a crystalline phase into the MG-matrix to form crystalline/amorphous nanolaminates (C/ANLs) [12–15], which utilize the size-dependent homogeneous plasticity of nanoscaled MGs as well as the inhomogeneous microstructure with isolated crystalline layers stabilizing the MGs against catastrophic failure. For example, the tensile ductility of 35 nm Cu/5 nm amorphous Cu-Zr multilayers can be sustained

* Corresponding author.
** Corresponding author.
*** Corresponding author.
E-mail addresses: jinyuzhang1002@mail.xjtu.edu.cn (J. Zhang), lgsammer@mail.xjtu.edu.cn (G. Liu), junsun@mail.xjtu.edu.cn (J. Sun).

https://doi.org/10.1016/j.jallcom.2018.07.177
0925-8388/

~13.8% with a high yield stress of ~1.09 GPa [12]. A large compressive deformability of >20% and a high strength of >1.5 GPa have been found in the uniaxial compression of Cu/Cu-Zr micropillars [16]. In these C/ANLs, the propagation, even the nucleation of SBs can be effectively suppressed by reducing the amorphous layer thickness and/or increasing the constraining effect by ultra-strong nanocrystals to improve their ductility and toughness [13,14,17]. Specifically, the crystalline/amorphous interfaces (CAIs) with weak shear strength play critical roles in plastic deformation of C/ANLs [12], as they serve as dislocation sources/sinks, but also manifest unique inelastic shear transfer characteristics, i.e., geometric compatibilities of the interfaces [18]. To achieve these improvements, careful control over the identity, volume fraction and size of the crystalline phases engineered within the MG-matrix is definitely required [10]. However, there is no general rule to guide such microstructure sensitive design in MG-matrix composites to achieve their optimized mechanical properties, in particular the effects of volume fraction of crystalline phase and different CAIs on fracture behaviors of MGs under tensile condition at nanoscale.

In addition, the intrinsically metastable nature renders MGs susceptible to transformation into more stable crystalline phases upon deformation, closely correlated with the stress state [19,20], sample size [21] and constraining condition [22,23]. Although extensive researches have been focused on exploiting the deformation-induced devitrification (DID) mechanisms and its influence on the mechanical behaviors of MGs and/or MG-based composites [24–26], there still are some discrepancies. For instance, some experimental results have revealed that DID in MG matrix could enable the dislocation-related work hardening to effectively hinder the propagation of SBs and prevent work softening [27,28], whereas others drew the opposite conclusion in deformed samples with a high volume fraction of crystallites [29,30]. However, neither the process of shear-induced viscous flow [25,27,31] nor the local temperature increase [32] in highly localized SBs for DID of MGs can eliminate this mentioned discrepancy yet. This is likely caused by the presence of the crystalline phase, which exerts a strong constraining effect on the amorphous phase. The most critical issue is thus whether or not the constraining effect derived from the adjacent crystalline layers induces the size- and constituent-dependence of DID during plastic deformation. Once this issue is resolved, it likely provides an explanation in terms of the fraction of nanocrystallites in MGs concerning the DID effects on plasticity of MG-matrix composites. This brings to the forefront that the kinetics of crystallization plays a central role in deforming MGs.

In this work, we aim to investigate the microstructural evolution (i.e., DID) in amorphous Cu-Zr nanolayers under different constraining effects from the neighboring crystalline Ag or Mo nanolayers, and how this crystallization influences the tensile ductility and fracture behavior of the two C/ANLs deposited on polyimide substrates. It is uncovered that the elastic modulus mismatch between constituents can be employed to guide the CAI design in the C/ANLs and control the occurrence of DID behavior. Below a critical (volume) fraction of nanocrystallites, it is of benefit to enhance the ductility *via* blocking the propagation of SBs by DID, above this, DID deteriorates the ductility. Our findings provide valuable insight into the understanding of deformation mechanism of nanoscaled MGs and the CAI design criterion from the perspective of constraining effects of crystalline phases for engineering ductile C/ANLs.

2. Experimental details

2.1. Material synthesis and characterization

The specimens used for uniaxial tensile testing are Ag/Cu-Zr and Mo/Cu-Zr C/ANLs with a constant modulation period λ ~100 nm (defined as the sum of the amorphous layer thickness h_A and the crystalline layer thickness h_C, $\lambda = h_A + h_C$) but different modulation ratios η ($\eta = h_A/h_C = 0.1–9.0$) deposited on the 125 μm-thick polyimide (Dupont Kapton®) substrates using magnetron sputtering at ambient temperature. Pure Cu (99.995%) and Zr (99.99%) targets (direct current sputtering) were employed to prepare the amorphous Cu-Zr nanolayers, and pure Ag (99.99%) and Mo (99.95%) targets (radio frequency sputtering) for the crystalline Ag and Mo nanolayers. Before the deposition process, the base pressure in the chamber was below 3.0×10^{-7} Torr, and the argon pressure was maintained to be 7.5×10^{-3} Torr during sputtering. The compositions of the Cu-Zr amorphous nanolayers are Cu75Zr25 and every C/ANLs has a total thickness of ~2.0 μm. Besides, the first layer deposited on the substrate was the amorphous Cu-Zr, and the cap layer was permanently a crystalline metal. High resolution transmission electron microscope (HRTEM) was performed on a JEOL JEM-2100F microscope for determining the microstructure of the specimens.

2.2. Uniaxial tensile testing

The mechanical properties of the polyimide-supported C/ANLs were evaluated by tensile testing at an identical strain rate of 1.0×10^{-4} s^{-1} *via* a Micro-Force Test System (MTS® Tytron 250) at ambient temperature. The gauge section of all specimens was 30 mm in length and ~4.0 mm in width. A critical macroscopic strain (ε_{cri}), representing formation of the microcrack on the macroscopic level, instead of the fracture strain or elongation, was utilized for characterizing the plastic deformability or ductility of the C/ANLs. Tensile testing associated with an electrical resistance change method has been developed to *in-situ* measure the ε_{cri} of the polymer-supported metal thin films [33]. Although the various crystalline constituent layers have different electrical resistivity, the relative change in electrical resistance of the films is highly remarkable before and after the initiation of microcracks. In addition, the plastic polyimide substrates with good elasticity are nonconducting completely and make no impact on the measurement of electrical performance. Therefore, this measured critical strain ε_{cri} can indeed reflect the inherent ductility of the C/ANLs without the influence of substrate of electrical resistivity. All specimens stretched to 10% strain were cross-sectioned and investigated *via* dual-beam focused ion beam (FIB) combined with scanning electron microscope (SEM) using an FEI microscope for analyzing the failure mechanism. The fracture angle θ, defined as the angle between the stress direction and the macrocrack direction, was utilized to characterize the fracture modes (e.g. opening and shearing fracture).

3. Results

3.1. Microstructure of the C/ANLs

The typical microstructures of as-deposited C/ANLs examined *via* HRTEM are presented in Fig. 1. One can clearly see the modulated layered structure with distinct CAIs between crystalline Ag or Mo and fully amorphous Cu-Zr nanolayers in the as-deposited C/ANLs, as displayed in Fig. 1(a)-(b). In addition, the Ag layers show columnar grains with the average grain size comparable to the layer thickness, while the Mo layers display undistinguished fine-columnar nanograins. The correspondingly selected area diffraction patterns (SADPs) in the inset of Fig. 1(a)-(b) definitely demonstrate polycrystalline diffraction spots with Ag (111), Ag (200), Ag (220) and Mo (110), Mo (200), Mo (211) textures, as well as the diffuse amorphous ring arising from the Cu-Zr nanolayers.

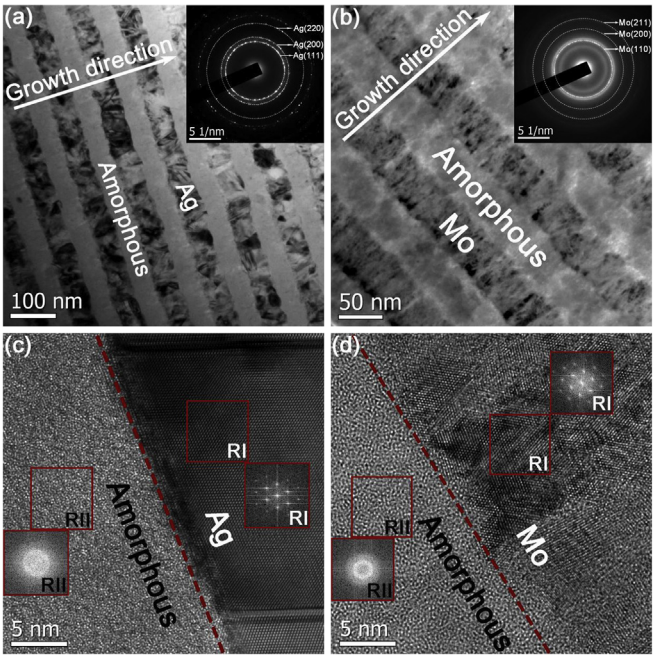

Fig. 1. Representative TEM and HRTEM images of as-deposited Ag/Cu-Zr (a, c) and Mo/Cu-Zr (b, d) C/ANLs with $\eta = 1.0$, respectively. The SADPs inserted in (a–b) exhibit the strong crystalline texture and diffuse amorphous rings. Fast Fourier transforms (FFTs) from two interesting regions RI (in the metal layer) and RII (in the Cu-Zr layer) in (c–d) indicate the crystalline and amorphous structure, respectively.

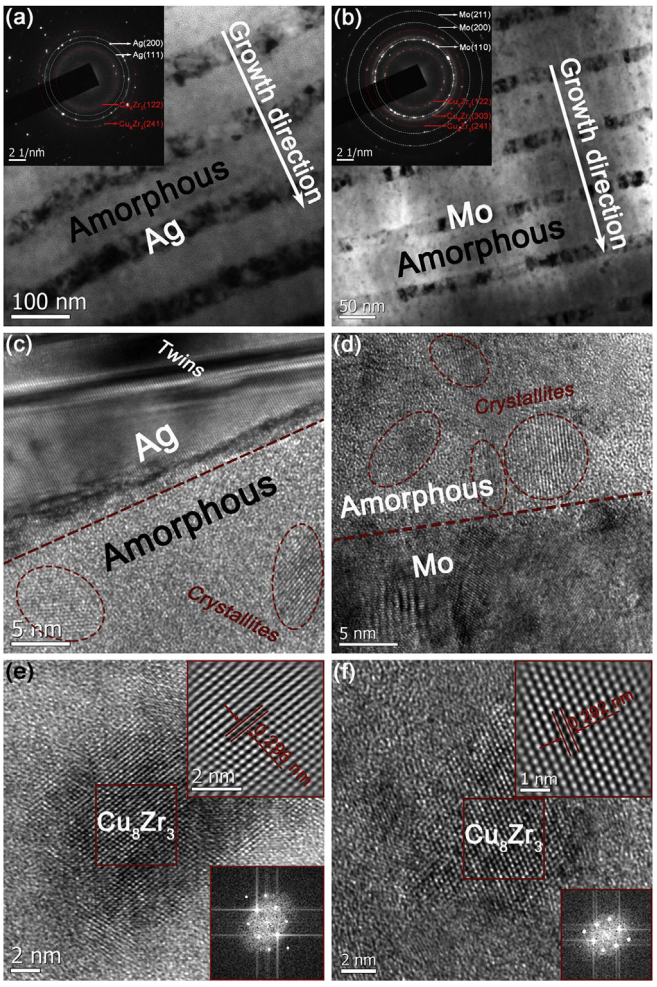

Fig. 2. Representative TEM and HRTEM images of Ag/Cu-Zr (a, c, e) and Mo/Cu-Zr (b, d, f) C/ANLs with $\eta = 3.0$ after tensile testing to 10% strain. There obviously exist a few nanocrystallites dispersed in the amorphous Cu-Zr nanolayer (indicated by the red dashed line in (c–d)). The FFT and inverse FFT results of boxed regions in (e–f) demonstrate the existence of a nanocrystalline Cu_8Zr_3 phase within the Cu-Zr nanolayer. (For interpretation of the references to colour in this figure legend, the reader is referred to the Web version of this article.)

Fig. 1(c)-(d) show the distinct CAIs in C/ANLs, and the fast Fourier transforms (FFTs) analyses indicate the crystalline structure in metal layers and the disordered amorphous structure in Cu-Zr layers.

To identify the crystallization behavior of the amorphous nanolayers during plastic deformation, cross-sectional TEM samples were fabricated from the 10% stretched C/ANLs to examine the microstructure features in detail. As shown in Fig. 2(a)-(b), the C/ANLs still retain their intact modulated structure with sharp interfaces. However, we can distinguish easily that dispersed precipitates of the orthogonal Cu_8Zr_3 phase are distributed in the deformed amorphous Cu-Zr layers in these two C/ANLs (see Fig. 2(c)-(d)), as supported by the newly emerged diffraction spots in the inserted SADPs (marked by red in Fig. 2(a)-(b)) and the FFTs & inverse FFTs analyses in Fig. 2(e)-(f). The stoichiometric ratio of Cu_8Zr_3 intermetallic is close to the chemical composition of the Cu75Zr25 amorphous nanolayers, implying a structural affinity between the amorphous Cu75Zr25 matrix and the precipitated Cu_8Zr_3 phase and no requirement of significant diffusion.

In addition, the average fraction and size of nanocrystallites that emerged in the amorphous Cu-Zr layers are measured statistically from the cross-sectional HRTEM images. More concretely, all the nanocrystallites are assumed to be spherical, and the area fraction instead of the volume fraction of nanocrystallites is calculated as $f_c = \sum_{i=1}^{n} A_{Ci}/A$, where n is the number of nanocrystallites in a selected area A, and A_C is the area of a nanocrystallite. Fig. 3 reveals that the crystallization percentage f_c in amorphous Cu-Zr nanolayers monotonically increases with reducing the modulation ratio η for both of the C/ANLs, indicating strong size-dependence of the DID. Moreover, the f_c value in Mo/Cu-Zr is about twice as large as that in Ag/Cu-Zr, while the nanocrystallites in Ag/Cu-Zr and Mo/Cu-Zr are roughly uniform in size with $d_c \sim 5$–9 nm.

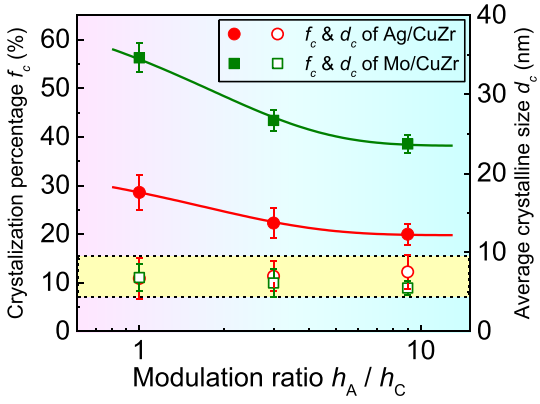

Fig. 3. Dependences of the crystallization percentage f_c and average crystallite size d_c of the nanocrystalline Cu_8Zr_3 phase on the modulation ratio η in the amorphous Cu-Zr layers of the two C/ANLs, respectively.

3.2. Tensile ductility of the C/ANLs

The C/ANLs are stretched to 10% strain to measure the critical strain ε_{cri} of nucleated microcrack(s) to characterize their tensile ductility [21,33]. Fig. 4 shows the tensile ductility (ε_{cri}) of the Ag/Cu-Zr (upper part) and Mo/Cu-Zr (lower part) C/ANLs as a function of η. It appears that the Ag/Cu-Zr C/ANLs exhibit a non-monotonic tensile ductility, i.e., ε_{cri} firstly reduces and then increases with raising η, reaching a minimum ε_{cri} at a critical modulation ratio η^* ~1.0. However, it is interesting to find that ε_{cri} monotonically increases with increasing η in the Mo/Cu-Zr C/ANLs, remarkably different from their Ag/Cu-Zr siblings. In addition, Ag/Cu-Zr C/ANLs exhibit a higher ε_{cri} than the Mo/Cu-Zr at a given η, which is related to the dislocation slips in different crystalline structures, i.e., FCC and BCC. This unusual η-dependence of the tensile ductility observed in these two C/ANLs likely stems from the constraining effect of the crystalline nanolayers on the amorphous Cu-Zr nanolayers and its related thickness-dependent DID behavior, which will be discussed in the next section.

3.3. Fracture behavior of the C/ANLs

The fracture behavior of C/ANLs is closely related to the deformation of constituent nanolayers and their constraining between each other. The cross-sectional microcrack morphologies of the 10%-stretched C/ANLs using the FIB are displayed for representative Ag/Cu-Zr and Mo/Cu-Zr C/ANLs along with their respective sketches in Fig. 5(a) and (b). From these cross-sectional observations inside a SEM, one can notice apparent necking in the Ag layers at η ~0.3, implying obvious plastic deformation of ductile Ag. A zigzag macrocrack inclined to the films/substrate interface with θ ~40° is finally created by multiple microcracks connected *via* ductile fracture of Ag layers. Actually, it can be seen from Fig. 5(a) that shearing fracture is evident for η below ~1.0, with fracture angles θ spanning from ~40° to 70° with increasing η to ~1.0, as shown in Fig. 6. Further increasing η, e.g. η ~3.0, obvious plastic deformation is generated in the amorphous Cu-Zr rather than the Ag nanolayers, and microcracks are mainly initiated in Ag layers, implying a brittle behavior of the crystalline Ag nanolayers with thickness below ~50 nm [33]. Accordingly, the fracture mode is then transformed to opening fracture with θ close to 90° (see Fig. 6).

However, unlike Ag nanolayers, the crystalline Mo nanolayers themselves are hard and brittle compared to the amorphous Cu-Zr layers. The SEM/FIB observations of Mo/Cu-Zr C/ANLs shown in Fig. 5(b) unveil that the brittle Mo nanolayers always fracture firstly [34] in the studied η-range at small strain due to the initiation of microcracks at the crystalline Mo layers. Additionally, the amorphous Cu-Zr nanolayers exhibit limited plastic deformation, implying that they cannot effectively block the propagation of microcracks initiated in Mo due to the strong stress field intensity. Thus, we always observe opening fracture for the whole range of η in Mo/Cu-Zr C/ANLs, seeing Fig. 5(b). Whereas, the fractural angle θ seems to show somewhat drop from ~90° at small η to ~82° at large η in the Mo/Cu-Zr C/ANLs, as shown in Fig. 6.

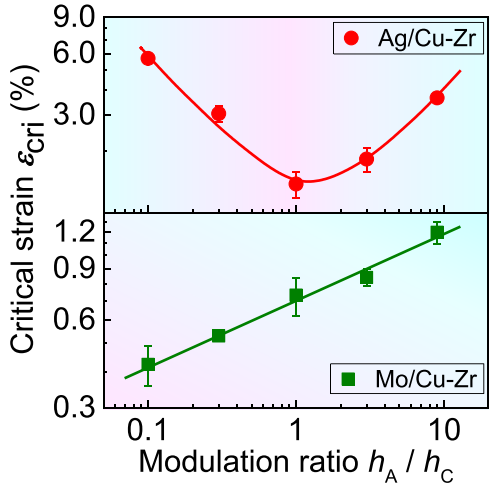

Fig. 4. Experimental measurements on the η-dependent tensile critical strain ε_{cri} of the Ag/Cu-Zr (upper part) and Mo/Cu-Zr C/ANLs (lower part).

4. Discussion

4.1. Size- and constituent-dependent DID

Previous studies have clearly demonstrated that DID of MGs can happen *via* stress-induced viscous flow during deformation in the absence of substantial temperature increase, which is strongly size- and stress state-dependent [21,25,31]. Specifically, our previous work has illuminated that the thickness-dependent DID was induced by the more STZs or atomic clusters in the thinner Cu-Zr films/layers, which could act as the embryo crystallites for DID [21]. In the present C/ANLs, we have to consider two heterogeneous materials bonded together at the atomic level to create a tightly contacted interface, i.e., the CAIs. Upon loading, the image force is unavoidably introduced in the C/ANLs due to the elastic modulus mismatch between these two constituents, which certainly contributes to the movement of dislocations near the CAIs at the nanoscale. During the plastic deformation, the amorphous Cu-Zr layers are certainly constrained by the neighboring crystalline layers, inducing the Koehler image force on the dislocations near to interface [35]. Assuming that a dislocation having Burgers vector b and a distance r from the CAI in crystalline layer, the resolved shearing stress required to drive the dislocation into the interface can be described as [35].

$$\tau_{image} = \frac{R\mu_C b \sin\theta}{4\pi r} \quad (1)$$

where $R = (\mu_A\text{-}\mu_C)/(\mu_A+\mu_C)$, μ_A and μ_C are the shear modulus of the amorphous and crystalline materials respectively, and θ is the smallest angle between the interface and the glide planes of crystal. The dislocation will be attracted from its image if R is negative, i.e., dislocations are susceptive to move across the CAI and be absorbed by the amorphous layer, inducing more STZ-mediated operations for the plasticity of amorphous layer. Conversely, a positive R implies that the dislocations are hard to move across the CAI into amorphous layer under the applied image force. Therefore, the DID in amorphous Cu-Zr is closely related to the elastic modulus of the crystalline counterparts.

For Ag/Cu-Zr C/ANLs, the emitted dislocations are inclined to stay/glide in Ag layers due to the positive image force caused by the smaller elastic modulus of Ag, thus the STZ-mediated plastic deformation in amorphous Cu-Zr is weakly enhanced by the dislocation interactions with the flow unit STZs, which could facilitate the subsequent DID behavior. However, for Mo/Cu-Zr C/ANLs, dislocations are strongly attracted by their images in the amorphous Cu-Zr layers because of the larger elastic modulus of Mo induced negative image force, and then a relatively large amount of STZs can be activated by the stimulation of absorbed dislocations for the nucleation of embryos, further promoting the crystallization behavior. In addition, DID can also be rationalized from the view of the stress field of an emitted dislocation, which is

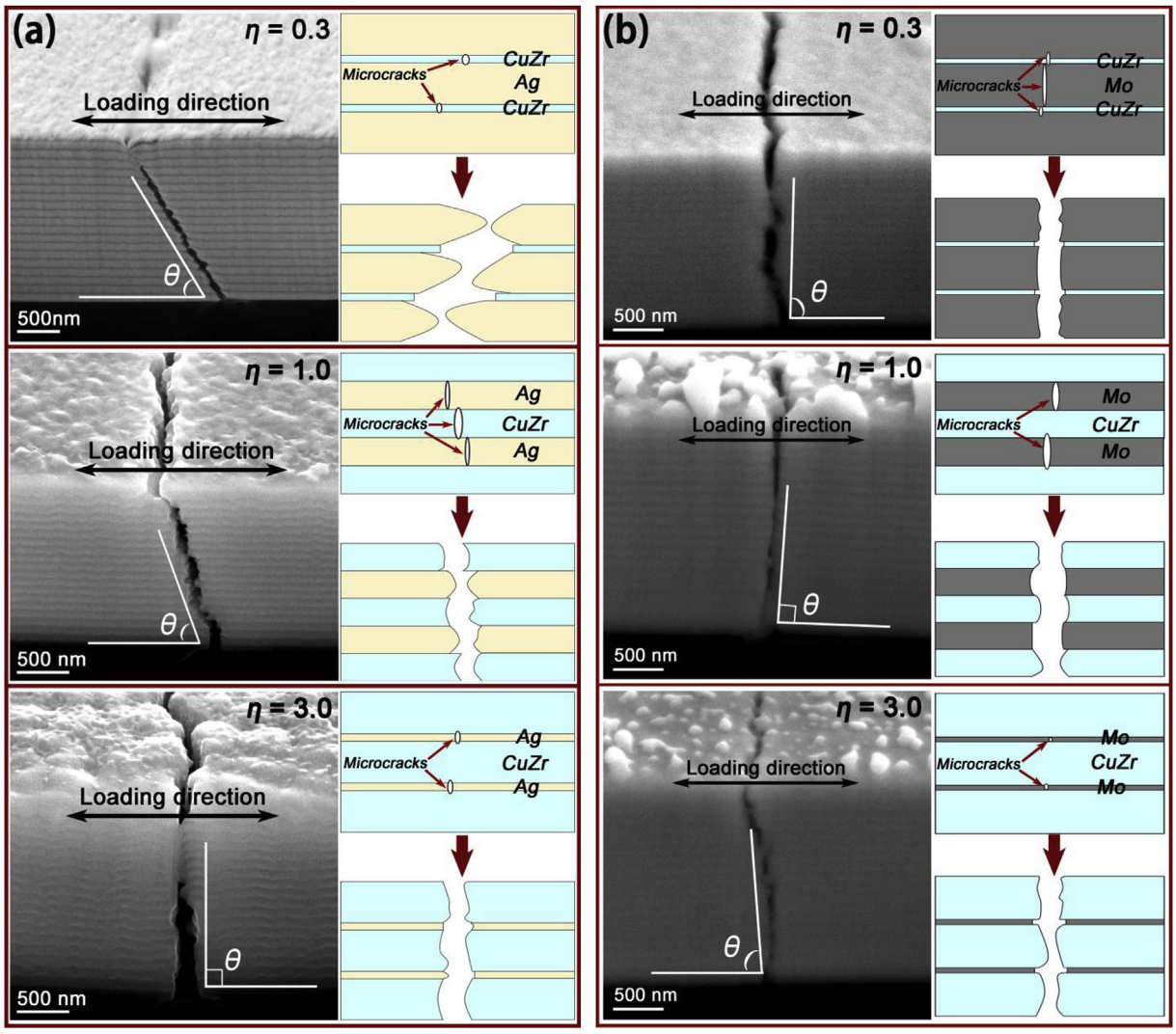

Fig. 5. Typical FIB cross-sectional images of the stretched Ag/Cu-Zr (a) and Mo/Cu-Zr (b) C/ANLs with $\eta = 0.3$, 1.0, and 3.0, respectively. Sketches of the fracture mechanisms are correspondingly given, showing a transition from shearing to opening fracture in Ag/Cu-Zr but an unchanged opening fracture in Mo/Cu-Zr C/ANLs.

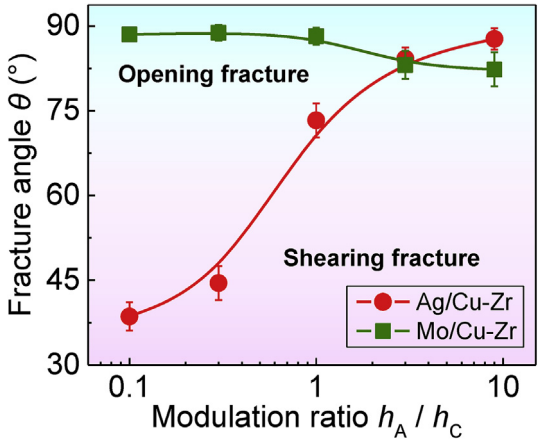

Fig. 6. Dependence of the fracture angle θ on the modulation ratio η in the two C/ANLs. The fracture mode transforms from shearing at small η to opening at large η for Ag/Cu-Zr, yet always remains unchanged opening fracture in Mo/Cu-Zr C/ANLs.

proportional to the product of shear modulus μ_C and magnitude of Burges vector b, i.e., $\mu_C b$. That is to say, a greater value of $\mu_C b$ leads to a stronger stress field. Once an emitted dislocation with a higher stress field runs into the amorphous Cu-Zr layer, it could attract more affinitive atoms in its stress field to adjust their positions for atomic rearrangements [36,37], stimulating more STZs to contribute to DID. Specifically, the dislocations could likely trigger different sizes of discrete STZs, in which those operative STZ sizes are dominated by the applied stress or the intensity of stress field [38]. In other words, for a given C/ANLs there will be a critical STZ size below which the STZs could rapidly relax comparing with the loading rate and make a contribution to the inelastic response, yet above which the STZs could essentially maintain their initial configuration unless the applied stress increases large enough to activate their rearrangement [39]. In Mo/Cu-Zr C/ANLs, the interatomic interactions in a stronger stress field can activate relatively more STZs but with smaller size, most of which can subsequently relax quickly and promote the diffusion motion of the constituent atoms. Thus, they will require less energy barrier for diffusion of an atom transporting from the amorphous matrix to the crystal nuclei or the precursor ordered clusters, inducing a higher nucleation rate for beneficial DID. By contrast, in Ag/Cu-Zr C/ANLs a relatively small amount of larger sized STZs can be triggered, most of which are difficult to activate relaxation and diffusion effectively. These

different micro-processes likely contribute to the observed discrepancies in the fractions and sizes of nanocrystallites in amorphous Cu-Zr nanolayers. Therefore, one can claim that the constituent dependent-modulus mismatch controls the DID propensity of different C/ANLs, and that STZ-mediated DID is more favorable to occur in stretched Mo/Cu-Zr C/ANLs at a given η.

The η-dependent DID can be understood in terms of the relative thickness or fraction of the constituents. Under the applied strain, the thicker crystalline layer could generate much more dislocations due to the included more sources or defect sites. That is to say, at a given C/ANLs, a greater thickness or fraction of metal nanolayers with lower flow stresses due to larger grains supplies more dislocations for the absorption by amorphous Cu-Zr nanolayers to activate more STZs, leading to a higher propensity of DID in the thinner amorphous Cu-Zr nanolayers. However, the monotonically η-dependent DID observed in the present experiment is probably caused by the fact that the stress field size is sufficiently smaller than the amorphous Cu-Zr layer thickness. Once the stress field size could be comparable or even larger than the amorphous layer thickness with decreasing η, there would be more dislocations annihilating in the thinner amorphous nanolayers [12], rendering more significant counterbalance of stress fields caused by dislocations with opposite sign. In such a case, the stress field effect of dislocations on DID could be remarkably suppressed, even no DID might occur. This scenario is consistent with the findings in the 35 nm Cu/5 nm Cu-Zr C/ANLs without DID [12].

4.2. Size- and constituent-dependent tensile fracture behavior

The Ag/Cu-Zr C/ANLs manifest a non-monotonic η-dependent ductility, while the fracture angle θ monotonically increases with η increasing from 0.1 to 9.0, namely, these C/ANLs are more prone to rupture in a shearing mode at smaller η and an opening mode at larger η. This is against the general belief that greater tensile ductility leads to smaller fracture angles in the form of shearing in nanolaminates [40,41]. By contrast, the Mo/Cu-Zr C/ANLs present a gradually reduced θ from ~90° to ~82° in the form of opening with slightly increased ε_{cri} with increasing η. These findings suggest that constraining effects of nanocrystalline metals on amorphous Cu-Zr can affect the microstructural evolution, thus influence the fracture behavior of C/ANLs.

4.2.1. The coupling effects of DID and constraining on the tensile ductility

Previous studies have uncovered that the ductility of monolithic crystalline thin films (e.g. Cu) decreases with reduction in film thickness, while the amorphous films just show the opposite trend [21]. In the C/ANLs, their size-dependent ductility becomes complicated due to the mutual constraining effects between the constituents. Microcracks would be nucleated in either the crystalline (Ag or Mo) nanolayers or the amorphous Cu-Zr nanolayers, relying on their relative ductility. However, the ductility of amorphous Cu-Zr nanolayers is significantly influenced by the DID process, thus affecting the nucleation sites of microcracks. As discussed before, the DID in amorphous Cu-Zr nanolayers is achieved by altering the stress field intensity of a dislocation caused by the modulus mismatch at the CAIs. In other words, a stronger stress field due to larger elastic mismatch is more favorable to promote DID. Therefore, the effect of the stress field of a dislocation on the microcrack nucleation is stronger in Mo/Cu-Zr and weaker in Ag/Cu-Zr at a given η.

For the Ag/Cu-Zr C/ANLs, their non-monotonic dependence of tensile ductility on the modulation ratio η (upper part of Fig. 4) can be understood in terms of DID and the mutual constraining effect between the crystalline and amorphous nanolayers. At small η ~0.1, the thicker ductile crystalline Ag nanolayers and the (possible) nanocrystallites in amorphous Cu-Zr nanolayers can suppress the propagation of microcracks initiated in the thinner amorphous Cu-Zr nanolayers [26,42], since the stress field intensity of the crack tip is quite weak, resulting in higher ductility in C/ANLs. However, at medium η (e.g. ~ 1.0), the crystalline Ag layers due to the insufficient volume become more brittle and harder to constrain the microcracks propagation [43], and simultaneously the amorphous Cu-Zr nanolayers with a higher fraction of nanocrystallites can only contribute limited ductility. In such a case, microcracks can simultaneously nucleate in both Ag and Cu-Zr nanolayers, rendering the minimum ductility of C/ANLs due to loss of the constraining effect. At large η ~9.0, the thicker amorphous Cu-Zr layers with the assistance of DID could impose a constraining effect on microcracks initiated in brittle crystalline Ag layers, thus exhibiting enhanced high ductility with further increasing η.

By contrast, for the Mo/Cu-Zr C/ANLs, a unilateral constraining effect is presented on the monotonic tensile ductility, shown as the lower part of Fig. 4. Because the crystalline Mo nanolayers themselves are hard and brittle compared with the Cu-Zr amorphous nanolayers, no mutual constraining effect is sustained. Instead, there is only an exclusive constraining effect of amorphous Cu-Zr on microcracks initiated in Mo layers in Mo/Cu-Zr C/ANLs. In such a case, microcracks will be always initiated in the brittle Mo nanolayers and propagate rapidly towards the CAI. At small η, the plastic amorphous Cu-Zr layer is so thin that it cannot block the propagation of microcracks, because the stress field intensity of the crack tip (proportional to the thickness of Mo layer) is large enough to overcome its shielding effect [41]. However, with increasing η, the plasticity of amorphous Cu-Zr nanolayers likely increases with the assistance of modest DID. Thus, the thicker amorphous Cu-Zr layers with enhanced plasticity can somewhat impede the microcrack propagation due to the coupling effects of the reduced stress field intensity of the crack tip in thin Mo layers and the nanocrystallites induced by DID in amorphous Cu-Zr layers. Therefore, a monotonic size-dependent ductility is observed in the Mo/Cu-Zr C/ANLs that increases with increasing η.

Generally, the activatable slip systems in FCC Ag are more than that in BCC Mo, implying that the Ag could be more ductile than Mo layers with the assistance of mobile dislocations for enhancing the plastic deformation. Upon tension, the Ag layers not only can manifest greater plastic deformability by the generation and migration of dislocations, but also block the shear steps in amorphous Cu-Zr layers through the CAIs, which play a vital role in transferring plasticity between the two constituents and trigger more homogeneous deformation in the amorphous Cu-Zr layers [44,45]. Thus, for a given C/ANLs, the Ag/Cu-Zr exhibited higher critical strain than that of Mo/Cu-Zr, as shown in Fig. 4. In addition, through the uniaxial tension of amorphous Cu-Nb single layer film and Cu/Cu-Nb C/ANLs with different constituent volume fraction on polyimide substrates, Fan et al. [43,45] investigated the constraint on amorphous layers by crystalline phase for enhancing the plasticity. They found that increasing the fraction of crystalline phase or decreasing the dimension of amorphous phase could effectively improve the critical strain or plasticity of C/ANLs, i.e., size-dependent tensile ductility, since a critical thickness of crystalline layer is required to impede the incipient SBs in Cu-Nb layers. Meanwhile, it was also demonstrated the transition of fracture surface morphology from brittle featureless to column-like and eventually ductile dimples (river patters) with increasing the volume fraction of Cu, corresponding to the transformation of fracture behavior from brittleness to ductility. In fact, this transformation was derived from the constraining effect of crystalline phase on the amorphous phase.

4.2.2. The coupling effects of DID and constraining on the fracture modes

The fracture angle θ in general reflects the constraining effect of the ductile phase on the brittle phase in nanolaminated materials. In crystalline/crystalline nanolaminates (C/CNLs), strong constraining of the ductile phase on the brittle phase often renders shearing fracture with θ approaching to 45° (in ductile nanolaminates), whereas weak constraining usually leads to opening fracture with θ approaching to 90° (in brittle nanolaminates) [41]. The tensile ductility and fracture angle are mutually exclusive to each other, i.e., the higher ductility the smaller the fracture angle is in C/CNLs, such as Cu/Zr, Cu/Nb and Cu/Cr [40,41]. However, in the present C/ANLs, two striking features different from that of C/CNLs are observed due to the occurrence of DID: (i) For Mo/Cu-Zr C/ANLs, the enhanced fracture strain relates to the reduced fracture angles, but the fracture mode remains opening in the studied η range. (ii) For Ag/Cu-Zr C/ANLs, higher ductility not only occurred with smaller fracture angles at $\eta < 1.0$, but also with larger fracture angles at $\eta > 1.0$. Next, we explain these two features in light of the coupling effects of DID and constraining.

Firstly, consider the effect of DID from the perspective of stress-affected zones (SAZ) of the crystalline particles, which could produce significant effects on the plasticity of C/ANLs and the propagation direction of microcracks. We can assume that every crystalline particle regularly embedded in the amorphous Cu-Zr nanolayers is surrounded by a SAZ of width w, spaced by the distance L to an adjacent SAZ. For the uniformly distributed nanocrystallites in the amorphous matrix, L can be expressed as $L = 1/\sqrt[3]{f_c/(\pi d_c^3/6)} - w$ by considering a cubic shape with a unit length, where f_c is the nanocrystallization fraction and d_c is the diameter of the nanocrystallite, see the sketches in Fig. 7(a). For a dilute nanocrystallite distribution ($L \geq w$), the shear bands are prone to propagate along the direction of maximum shear stress (~45°), since the spacing L is large enough so that the SAZs cannot produce interaction with the shear bands to disturb their propagation, therefore the nanocrystallites almost have no blocking effect on the propagation of shear bands. This situation is consistent with the shear fracture mode of single layer amorphous Cu-Nb films through the formation of SBs [43]. While for a larger population of SAZs ($w > L > 0$), the shear bands would repeatedly deflect from the maximum shear stress direction under the influence of SAZs. Consequently, the ductility of the amorphous nanolayer will be enhanced under this condition and the fracture angle is larger than 45° but smaller than 90°, as displayed in Fig. 7(a). As the crystallization behavior aggravates so that the SAZs start to overlap, i.e. $L \leq 0$, the shear bands affected by SAZs will be prone to propagate confined through these weakest regions between two adjacent SAZs, oriented along the direction almost perpendicular to the loading axis. Taken together, as shown in Fig. 7(b), the shearing fracture of an amorphous layer occurs in region I and II with the corresponding fracture angle θ spanning from ~45° to ~90°, and the opening fracture prevails in region III with $\theta \sim 90°$. However, the enhancement of ductility due to DID only occurs in region II.

In what follows, we elucidate the fracture of the two C/ANLs based on this concept. For the Ag/Cu-Zr C/ANLs, as shown in

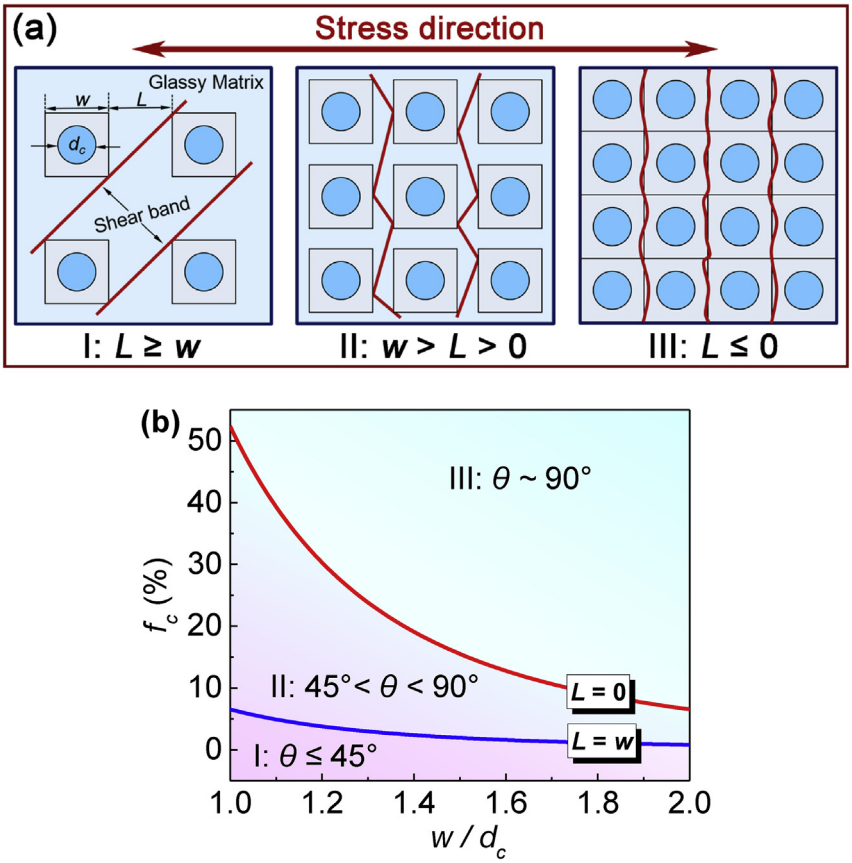

Fig. 7. (a) Schematic diagram on the propagation direction of the microcracks at different size L in the amorphous nanolayer. The fracture angle θ is prone to align along the direction of maximum shear stress ($\theta \sim 45°$) at $L \geq w$, $\theta \sim 90°$ as the SAZs begin to overlap ($L \leq 0$), and in between for $w > L > 0$. (b) The variation of the calculated crystallization percentage f_c with the ratio of the SAZ size w to the crystallites size d_c at $L = w$ (blue solid line) and $L = 0$ (red solid line). (For interpretation of the references to colour in this figure legend, the reader is referred to the Web version of this article.)

Fig. 5(a), at large η ~9.0, the thicker amorphous Cu-Zr layers with relatively smaller crystallization percentage f_c exhibit ductile shearing deformation, while the microcracks initiated in the thinner crystalline Ag layers could propagate slowly into the amorphous layers almost without suffering from blocking effects of nanocrystallites. Once the amorphous Cu-Zr layer is unable to balance the growing energy ahead of the microcrack tip upon progressively applied stresses, the microcracks will penetrate into the Cu-Zr layers and trigger opening fracture with angle θ close to 90°, but apparent tensile ductility. By contrast, the amorphous Cu-Zr nanolayers at η ~1.0 exhibit limited plastic deformation capacity associated with excessive DID, while the crystalline layers still could initiate microcracks easily at this size. These two factors along with the weak blocking effect of nanocrystallites render a slightly inclined shearing fracture angle (~72°) but inferior ductility in C/ANLs. For the small η ~0.1, the propagation of microcracks initiated in the thinner/brittle Cu-Zr nanolayers is shielded by the thicker/soft crystalline nanolayers, which exhibit evident plastic deformation, finally resulting in a typical shearing fracture with θ ~45°. Considering the Mo/Cu-Zr C/ANLs, due to the exorbitant DID behavior in the amorphous Cu-Zr layers ($L \leq 0$) and the brittle crystalline Mo layers, there will always be opening fracture mode at different η (see Fig. 5(b)), accompanying poor ductility. Therefore, although the amorphous Cu-Zr layers in Mo/Cu-Zr present more significant DID, the nanocrystallites in the amorphous Cu-Zr layers likely weaken the plasticity for the structural inhomogeneity once the volume fraction of nanocrystallites is above a certain level [29,46], referring to Fig. 7. Actually, severe nanocrystallization would induce a reduction in free volume in amorphous Cu-Zr layers, which in turn renders the disordered amorphous layers lose the capability for cooperative plastic flow. Particularly, when excessive nanocrystallites are distributed in the amorphous layers, microcracks are prone to initiate at the weakest overlapping regions of the SAZs [46], deteriorating the ductility. Instead, the moderate nanoparticles formed during the subsequent deformation of amorphous Cu-Zr layers not only release the internal stress, but also blunt the crack tips to obstruct their further propagation [26], facilitating improvement of plasticity.

5. Conclusions

This work systematically investigated the microstructure evolution, tensile ductility and fracture mode of Ag/Cu-Zr and Mo/Cu-Zr crystalline/amorphous nanolaminates (C/ANLs) under different constituent constraining conditions. Experimental results demonstrate that the deformation-induced devitrification (DID) in C/ANLs is tunable *via* controlling the elastic modulus mismatch between the constituent materials and the amorphous layer thickness. This DID mechanism is qualitatively elucidated in terms of the stress field of an emitted dislocation near the CAIs and the image force between the constituents.

The fracture behavior of the C/ANLs is closely related to the DID process in amorphous Cu-Zr layers and the constraining effects between constituent nanolayers. The DID marginally emerging in the C/ANLs systems with small elastic modulus mismatch could promote their subsequent plasticity due to the effective blocking of the nanocrystallites in amorphous Cu-Zr layers and the ductile crystalline layers on microcracks, such as Ag/Cu-Zr. However, the DID prominently emerging in the C/ANLs with large elastic modulus mismatch deteriorates their subsequent plasticity because of the inferior constraining effect of the excessive nanocrystallites and the brittle crystalline layers, such as Mo/Cu-Zr. Our findings provide a valuable avenue to design high performance crystalline/amorphous composites from the perspective of the constraining effect of a crystalline on the amorphous phase.

Acknowledgements

This work was supported by the National Natural Science Foundation of China (Grant Nos. 51621063, 51625103, 51790482, 51761135031, 51722104 and 51571157), the National Key Research and Development Program of China (2017YFB0702301) and the 111 Project of China (B06025). This work is also supported by the International Joint Laboratory for Micro/Nano Manufacturing and Measurement Technologies. JYZ is grateful for the Fok Ying Tong Education Foundation (161096), China Postdoctoral Science Foundation (2016M590940, 2017T100744) Shaanxi Province Postdoctoral Scientific Research Projects (2016BSHEDZZ09) for part of financial support. KW thanks the support from the China Postdoctoral Science Foundation (2016M602811). YQW thanks for the financial support from the China Scholarship Council (CSC, 201606280056).

References

[1] C. Schuh, T. Hufnagel, U. Ramamurty, Mechanical behavior of amorphous alloys, Acta Mater. 55 (2007) 4067–4109.
[2] J.R. Greer, J.T.M. De Hosson, Plasticity in small-sized metallic systems: intrinsic versus extrinsic size effect, Prog. Mater. Sci. 56 (2011) 654–724.
[3] M.M. Trexler, N.N. Thadhani, Mechanical properties of bulk metallic glasses, Prog. Mater. Sci. 55 (2010) 759–839.
[4] Y.Q. Cheng, E. Ma, Atomic-level structure and structure–property relationship in metallic glasses, Prog. Mater. Sci. 56 (2011) 379–473.
[5] A.L. Greer, Y.Q. Cheng, E. Ma, Shear bands in metallic glasses, Mater. Sci. Eng. R 74 (2013) 71–132.
[6] S. Pauly, S. Gorantla, G. Wang, U. Kuhn, J. Eckert, Transformation-mediated ductility in CuZr-based bulk metallic glasses, Nat. Mater. 9 (2010) 473–477.
[7] L. Tian, Y.Q. Cheng, Z.W. Shan, J. Li, C.C. Wang, X.D. Han, J. Sun, E. Ma, Approaching the ideal elastic limit of metallic glasses, Nat. Commun. 3 (2012) 609.
[8] X. Zhou, C. Chen, Strengthening and toughening mechanisms of amorphous/amorphous nanolaminates, Int. J. Plast. 80 (2016) 75–85.
[9] J. Das, M. Tang, K. Kim, R. Theissmann, F. Baier, W. Wang, J. Eckert, "Work-Hardenable" ductile bulk metallic glass, Phys. Rev. Lett. 94 (2005), 205501.
[10] X. Tong, G. Wang, J. Yi, J.L. Ren, S. Pauly, Y.L. Gao, Q.J. Zhai, N. Mattern, K.A. Dahmen, P.K. Liaw, J. Eckert, Shear avalanches in plastic deformation of a metallic glass composite, Int. J. Plast. 77 (2016) 141–155.
[11] D.C. Hofmann, J.Y. Suh, A. Wiest, M.L. Lind, M.D. Demetriou, W.L. Johnson, Development of tough, low-density titanium-based bulk metallic glass matrix composites with tensile ductility, Proc. Natl. Acad. Sci. U. S. A. 105 (2008) 20136–20140.
[12] Y. Wang, J. Li, A.V. Hamza, T.W. Barbee Jr., Ductile crystalline-amorphous nanolaminates, Proc. Natl. Acad. Sci. U.S.A. 104 (2007) 11155–11160.
[13] A. Donohue, F. Spaepen, R.G. Hoagland, A. Misra, Suppression of the shear band instability during plastic flow of nanometer-scale confined metallic glasses, Appl. Phys. Lett. 91 (2007), 241905.
[14] W. Guo, E.A. Jägle, P.-P. Choi, J. Yao, A. Kostka, J.M. Schneider, D. Raabe, Shear-induced mixing governs codeformation of crystalline-amorphous nanolaminates, Phys. Rev. Lett. 113 (2014), 035501.
[15] Z.-D. Sha, P.S. Branicio, H.P. Lee, T.E. Tay, Strong and ductile nanolaminate composites combining metallic glasses and nanoglasses, Int. J. Plast. 90 (2017) 231–241.
[16] J.Y. Zhang, G. Liu, S.Y. Lei, J.J. Niu, J. Sun, Transition from homogeneous-like to shear-band deformation in nanolayered crystalline Cu/amorphous Cu–Zr micropillars: intrinsic vs. extrinsic size effect, Acta Mater. 60 (2012) 7183–7196.
[17] J.-Y. Kim, D. Jang, J.R. Greer, Nanolaminates utilizing size-dependent homogeneous plasticity of metallic glasses, Adv. Funct. Mater. 21 (2011) 4550–4554.
[18] I.J. Beyerlein, M.J. Demkowicz, A. Misra, B.P. Uberuaga, Defect-interface interactions, Prog. Mater. Sci. 74 (2015) 125–210.
[19] W.H. Jiang, M. Atzmon, The effect of compression and tension on shear-band structure and nanocrystallization in amorphous Al90Fe5Gd5: a high-resolution transmission electron microscopy study, Acta Mater. 51 (2003) 4095–4105.
[20] Y. Liu, J. Jian, J.H. Lee, C. Wang, Q.P. Cao, C. Gutierrez, H. Wang, J.Z. Jiang, X. Zhang, Repetitive ultra-low stress induced nanocrystallization in amorphous Cu–Zr–Al alloy evidenced by in situ nanoindentation, Mater. Res. Lett. 2 (2014) 209–216.
[21] Y.Q. Wang, J.Y. Zhang, X.Q. Liang, K. Wu, G. Liu, J. Sun, Size- and constituent-dependent deformation mechanisms and strain rate sensitivity in nanolaminated crystalline Cu/amorphous Cu–Zr films, Acta Mater. 95 (2015) 132–144.
[22] Z.M. Wang, J.Y. Wang, L.P.H. Jeurgens, E.J. Mittemeijer, Thermodynamics and mechanism of metal-induced crystallization in immiscible alloy systems:

experiments and calculations on Al/a-Ge and Al/a-Si bilayers, Phys. Rev. B 77 (2008), 045424.
[23] Z.M. Wang, J.Y. Wang, L.P.H. Jeurgens, E.J. Mittemeijer, Tailoring the ultrathin Al-Induced crystallization temperature of amorphous Si by application of interface thermodynamics, Phys. Rev. Lett. 100 (2008).
[24] J.-C. Lee, Y.-C. Kim, J.-P. Ahn, H.-S. Kim, S.-H. Lee, B.-J. Lee, Deformation-induced nanocrystallization and its influence on work hardening in a bulk amorphous matrix composite, Acta Mater. 52 (2004) 1525–1533.
[25] S.-W. Lee, M.-Y. Huh, S.-W. Chae, J.-C. Lee, Mechanism of the deformation-induced nanocrystallization in a Cu-based bulk amorphous alloy under uni-axial compression, Scripta Mater. 54 (2006) 1439–1444.
[26] J.Y. Zhang, G. Liu, J. Sun, Self-toughening crystalline Cu/amorphous Cu–Zr nanolaminates: deformation-induced devitrification, Acta Mater. 66 (2014) 22–31.
[27] M. Chen, A. Inoue, W. Zhang, T. Sakurai, Extraordinary plasticity of ductile bulk metallic glasses, Phys. Rev. Lett. 96 (2006), 245502.
[28] S. Pauly, G. Liu, G. Wang, U. Kühn, N. Mattern, J. Eckert, Microstructural heterogeneities governing the deformation of Cu47.5Zr47.5Al5 bulk metallic glass composites, Acta Mater. 57 (2009) 5445–5453.
[29] Y.C. Kim, J.H. Na, J.M. Park, D.H. Kim, J.K. Lee, W.T. Kim, Role of nanometer-scale quasicrystals in improving the mechanical behavior of Ti-based bulk metallic glasses, Appl. Phys. Lett. 83 (2003) 3093.
[30] Z.Q. Liu, G. Liu, R.T. Qu, Z.F. Zhang, S.J. Wu, T. Zhang, Microstructural percolation assisted breakthrough of trade-off between strength and ductility in CuZr-based metallic glass composites, Sci. Rep. 4 (2014) 4167.
[31] J.J. Kim, Y. Choi, S. Suresh, A.S. Argon, Nanocrystallization during nano-indentation of a bulk amorphous metal alloy at room temperature, Science 295 (2002) 654–657.
[32] J.J. Lewandowski, A.L. Greer, Temperature rise at shear bands in metallic glasses, Nat. Mater. 5 (2005) 15–18.
[33] R.M. Niu, G. Liu, C. Wang, G. Zhang, X.D. Ding, J. Sun, Thickness dependent critical strain in submicron Cu films adherent to polymer substrate, Appl. Phys. Lett. 90 (2007), 161907.
[34] T. Jörg, M.J. Cordill, R. Franz, C. Kirchlechner, D.M. Többens, J. Winkler, C. Mitterer, Thickness dependence of the electro-mechanical response of sputter-deposited Mo thin films on polyimide: insights from in situ synchrotron diffraction tensile tests, Mater. Sci. Eng., A 697 (2017) 17–23.
[35] J.S. Koehler, Attempt to design a strong solid, Phys. Rev. B 2 (1970) 547–551.
[36] J.Y. Zhang, G. Liu, J. Sun, Crystallization-aided extraordinary plastic deformation in nanolayered crystalline Cu/amorphous Cu-Zr micropillars, Sci. Rep. 3 (2013) 2324.
[37] B. Cheng, J.R. Trelewicz, Mechanistic coupling of dislocation and shear transformation zone plasticity in crystalline-amorphous nanolaminates, Acta Mater. 117 (2016) 293–305.
[38] H. Gao, L. Zhang, S.P. Baker, Dislocation core spreading at interfaces between metal films and amorphous substrates, J. Mech. Phys. Solid. 50 (2002) 2169–2202.
[39] T.C. Hufnagel, C.A. Schuh, M.L. Falk, Deformation of metallic glasses: recent developments in theory, simulations, and experiments, Acta Mater. 109 (2016) 375–393.
[40] J.Y. Zhang, X. Zhang, G. Liu, G.J. Zhang, J. Sun, Scaling of the ductility with yield strength in nanostructured Cu/Cr multilayer films, Scripta Mater. 63 (2010) 101–104.
[41] J.Y. Zhang, X. Zhang, R.H. Wang, S.Y. Lei, P. Zhang, J.J. Niu, G. Liu, G.J. Zhang, J. Sun, Length-scale-dependent deformation and fracture behavior of Cu/X (X=Nb, Zr) multilayers: the constraining effects of the ductile phase on the brittle phase, Acta Mater. 59 (2011) 7368–7379.
[42] N. Li, H. Wang, A. Misra, J. Wang, In situ nanoindentation study of plastic co-deformation in Al-TiN nanocomposites, Sci. Rep. 4 (2014) 6633.
[43] Z. Fan, Q. Li, J. Li, S. Xue, H. Wang, X. Zhang, Tailoring plasticity of metallic glasses via interfaces in Cu/amorphous CuNb laminates, J. Mater. Res. 32 (2017) 2680–2689.
[44] C. Brandl, T.C. Germann, A. Misra, Structure and shear deformation of metallic crystalline–amorphous interfaces, Acta Mater. 61 (2013) 3600–3611.
[45] Z. Fan, J. Li, Y. Yang, J. Wang, Q. Li, S. Xue, H. Wang, J. Lou, X. Zhang, "Ductile" fracture of metallic glass nanolaminates, Adv. Mater. Interfaces 4 (2017), 1700510.
[46] B.A. Sun, K.K. Song, S. Pauly, P. Gargarella, J. Yi, G. Wang, C.T. Liu, J. Eckert, Y. Yang, Transformation-mediated plasticity in CuZr based metallic glass composites: a quantitative mechanistic understanding, Int. J. Plast. 85 (2016) 34–51.